Crystal structure and phase transitions of sodium potassium niobate perovskites

Jenny Tellier, B. Malic, B. Dkhil, D. Jenko, J. Cilensek, M. Kosec

Crystal structure and phase transitions of sodium potassium niobate perovskites

J. Tellier[1], B. Malic[1], B. Dkhil[2], D. Jenko[1], J. Cilensek[1], M. Kosec[1]

[1] *Jozef Stefan Institute, Jamova 39, 1000 Ljubljana, Slovenija*

[2] *Laboratoire Structures, Propriétés et Modélisation des Solides, CNRS-UMR 8580, Ecole Centrale Paris, Grande voie des vignes, 92925 Châtenay-Malabry, France*

Abstract

This paper presents the crystal structure and the phase transitions of $K_xNa_{1-x}NbO_3$ ($0.4 \leq x \leq 0.6$). X-ray diffraction measurements were used to follow the change of the unit-cell parameters and the symmetry in the temperature range 100–800K. At room temperature all the compositions exhibited a monoclinic metric of the unit cell with a small monoclinic distortion ($90.32° \leq \beta \leq 90.34°$). No major change of symmetry was evidenced in the investigated compositional range, which should be characteristic of the morphotropic phase-boundary region. With increasing temperature, the samples underwent first-order monoclinic-tetragonal and tetragonal-cubic transitions. Only the potassium-rich phases were rhombohedral at 100 K.

Keywords

KNN, crystal structure, phase transitions, X-Ray diffraction, Rietveld method.

Corresponding author: jenny.tellier@ijs.si

Introduction

Solid solutions based on sodium potassium niobate ($K_xNa_{1-x}NbO_3$) are promising candidates for lead-free piezoelectric ceramics. In this system, the best dielectric and piezoelectric properties were found for the compositions with x=0.5 [1] or x=0.48 [2]. The optimum dielectric response in this system is reported [3] for the composition $K_{0.475}Na_{0.525}NbO_3$, which corresponds to the morphotropic phase boundary, evidenced by Tennery et al. [4].

Although it is well known that the properties of this system are closely related to the composition, not much information is available on the structure and the symmetry of these perovskites.

The phase diagram of $K_xNa_{1-x}NbO_3$ [3] shows only a small part related to the $NaNbO_3$ symmetry. Only 2% of potassium in the composition is sufficient to change the initial structure, based on $NaNbO_3$, towards one based on $KNbO_3$. Ahtee and Hewat found, using neutron diffraction, that the structure of x=0.02 and x=0.1 could be refined as a perovskite with a monoclinic symmetry [5]. They also pointed out that for these two compositions, the difference between the monoclinic and orthorhombic structure is small.

This may be the reason why many publications report the use of an orthorhombic metric for the refinements of the cell parameters of $K_{0.5}Na_{0.5}NbO_3$ at room temperature. Some of them use orthorhombic parameters $a \approx c \approx 4\sqrt{2}$ Å and $b \approx 4$ Å, or even $a \approx b \approx c \approx 4$ Å [6-8]. Shirane et al. used monoclinic cell parameters to describe and refine a selection of $K_xNa_{1-x}NbO_3$ structures in the range x = [0–1], but they later transformed it into the corresponding orthorhombic metric for an easier comparison with tetragonal and cubic phases [9]. However, this is not in agreement with the monoclinic unit-cell parameters and the Pm space group defined by Shiratori et al. using Raman spectroscopy [10].

An additional triclinic symmetry has been reported [10, 11] for the special case of very small particles of about 130 nm. According to the authors, this triclinic symmetry is probably due to the cationic ordering of potassium and sodium in the unit cell, induced by the very small number of cells in the particle.

The temperatures of the phase transitions in $K_xNa_{1-x}NbO_3$ have already been determined using electrical measurements by Egerton *et al.* [1]. The studied compositions are reported to have phase-transition temperatures in the same range as $KNbO_3$, but no systematic work can be found on this subject. Ahtee and Glazer [12, 13] described the octahedral tilting system in some of these perovskites at different temperatures in order to complete the phase diagram.

Substituted KNN was studied by Takeda *et al.* [14]. The perovskite $(Ag_{0.75}Li_{0.1}Na_{0.1}K_{0.05})NbO_3$ is shown to exhibit a rhombohedral → monoclinic → tetragonal → cubic transition. In contrast to the other transitions, the rhombohedral → monoclinic transition is gradual in this compound.

This work is a systematic study of the evolution of the unit-cell parameters of $K_xNa_{1-x}NbO_3$ compounds in the range x= [0.4-0.6] at room temperature and between 100 K and 800 K. The aim was to establish whether differences in the symmetry exist in these perovskites on both sides of the morphotropic phase boundary which was evidenced by Tennery *et al.* [4]. The phase transitions were followed from the high-temperature cubic to the low-temperature distorted perovskite. For this study the cubic, tetragonal, monoclinic and rhombohedral phases were selected for the different temperatures. All these unit cells have parameters of about 4Å and thus can be directly compared.

Experimental

The starting compounds $NaNbO_3$ and $KNbO_3$ were prepared from Na_2CO_3 (Aldrich 99.95–100.05%), K_2CO_3 (Aldrich 99+%) and Nb_2O_5 (Aldrich 99.9%). Prior to weighing the powders in the stoichiometric ratio, Na_2CO_3 and K_2CO_3 were dried for 2h at 200°C in an oven to remove the adsorbed water from these hygroscopic materials. The oxide and carbonate were then mixed using acetone as a liquid medium and then dried at 200°C prior to calcination. The powders were annealed twice with intermediate milling: the first time at 650°C for 4h and the second time at 700°C for 4h, to obtain pure perovskite

The $K_xNa_{1-x}NbO_3$ (x = 0.4, 0.42, 0.44, 0.46, 0.475, 0.48, 0.5, 0.52, 0.54, 0.56, 0.58 and 0.6) powders were prepared by mixing $NaNbO_3$ and $KNbO_3$. The stoichiometric compositions were mixed in an atritor using acetone as the liquid medium. After drying at 200°C, the powders are uniaxially pressed into pellets (diameter 8 mm) with an applied pressure of 50 MPa, annealed at 1100°C for 4h, and milled in an agate mortar.

This method of preparation was chosen in order to avoid the formation of compounds of the systems Na_2O–Nb_2O_5 and K_2O–Nb_2O_5 that do not belong to the perovskite phase, such as those listed by Irle et al. [15].

The samples for differential scanning calorimetry (DSC) were pressed uniaxially (diameter 8 mm) with an applied pressure of 50 MPa. Then the pellets were annealed at 1100°C for 4 hours. The DSC curves were recorded on a Netzsch DSC 204 with a temperature ramp of 10°C per minute. The temperatures of the phase transitions were measured at the onset of the peaks.

X-ray diffractograms were recorded at room temperature on a PANalytical X'Pert PRO diffractometer (Cu $K_{\alpha 1}$, Ge monochromator) with an angular range of 5–85° using a 0.016° step and 100s per step. These conditions ensured the good quality of the pattern to check the purity and the structural details of the synthesized compounds.

A two-axis diffractometer in Bragg-Brentano geometry with Cu K_β radiation was used for the low- and high-temperature recording. The control of the temperature was provided either by a cryostat, between 100K and 300K, or a separate furnace, from 300K to 800K. Selected reflections, corresponding to the pseudo-cubic (200), (220) and (222) families, were measured in order to shorten the time of the experiment. These three major reflections were indeed sufficient to see the changing of the parameters and the symmetry in KNN with increasing temperature.

The cell parameters were refined using Jana2000 software [16]. This performs a full-pattern matching using the Rietveld method. The unit-cell parameters a, b, c and β were refined. A shift correction was made in order to obtain the correct zero position. The background was modelled using the Legendre polynom and the peaks' profiles were refined using a pseudo-Voigt function. The chosen space groups for these refinements for monoclinic, tetragonal and cubic phases were Pm (SG n°6), P4mm (SG n°99) and Pm-3m (SG n°221) [17] respectively.

Results

All the studied compositions of the solid solution crystallised in a pure perovskite phase with the applied thermal treatment. All the reflexions could be indexed with JCPDS n° 77-0038 ($K_{0.65}Na_{0.35}NbO_3$) after a slight change of cell parameters to adjust the positions (see the example of $K_{0.5}Na_{0.5}NbO_3$ in Figure 1). There was no evidence of a cationic ordering as no superstructure can be seen in the diagram. No trace of the starting perovskites ($NaNbO_3$ and $KNbO_3$) can be found in the diagrams.

XRD Investigation at room temperature

Since the beginning of the studies the $K_xNa_{1-x}NbO_3$ solid solution in the range x = [0.4–0.6] has been described using different unit-cell parameters at room temperature. It is thus possible to express the metric of these compounds with either monoclinic ($a \approx b \approx c \approx 4$ Å, $\beta \approx 90.3°$) or orthorhombic ($a \approx c \approx 4\sqrt{2}$ Å and $b \approx 4$ Å) unit cells, with a change in the indexes. The relationship between the monoclinic and the orthorhombic unit cells is shown in Figure 2. In our case, the cell parameters were chosen so as to have a more direct comparison with the cubic high-temperature phase. At room temperature all the refinements were made with monoclinic parameters and the Pm space group (SG n°6), and the results are presented in Table 1 and Figure 3.

The unit-cell parameters a, b and c increased regularly with the increasing content of potassium, while the beta angle decreased towards 90°, and thus to a more symmetrical orthorhombic unit cell. It is interesting to note that this decrease is not regular; a change of slope in the decrease of the β angle is visible on the K-rich side of the phase diagram.

The unit-cell volume was refined for each compound from the X-ray diffraction diagram (see the values in Table 1). The result (Figure 4) shows a linear evolution of the volume with the composition, following Vegard's law. This linear increase in volume is in agreement with the existence of a solid solution, and shows that the different perovskites synthesised are of the correct composition. With an increasing content of K^+ (r = 1.64 Å in XII coordination [18]) instead of Na^+ (r = 1.39 Å in XII coordination), the volume of the unit cell increases logically.

High-temperature phase transitions

The phase transitions were determined by differential scanning calorimetry (DSC), and the temperatures are given in Table 2. The endothermic peaks on heating related to the first-order transitions are clearly visible at these temperatures.

The transition temperatures increased with an increasing content of potassium (see Figure 5). For the first transition (monoclinic-tetragonal) this increase was regular. For the second one (tetragonal-cubic) a discontinuity was observed for the compositions $K_{0.475}Na_{0.525}NbO_3$ to $K_{0.5}Na_{0.5}NbO_3$, where the temperature decreased, before increasing again regularly.

The two high-temperature transitions were followed by tracking the change of the unit-cell parameters as a function of temperature. The unit-cell parameters were refined for each temperature by a pattern matching on three families of reflections, (200), (220) and (222). The results obtained are comparable for every composition, with a change in the temperature scale. The temperatures of the transitions were in agreement with those measured with DSC. The results obtained for the composition $K_{0.56}Na_{0.44}NbO_3$ are given here as an example in Figure 6, Figure 7, Figure 8 and Figure 9.

For all the compositions, the thermal evolution of the cell parameters was continuous in the monoclinic, tetragonal and cubic phases. At the transition temperatures, an abrupt change occurred, and a mixing of the monoclinic and tetragonal, or the tetragonal and cubic, was observed (Figure 6). This abrupt change of unit-cell parameters and phase mixing is in agreement with the first-order character of the transitions. The mixing of phases at the transitions is visible in Figure 7. The diffraction patterns show both series of (200) and (220) reflections, which make it possible to distinguish the monoclinic, tetragonal and cubic symmetries. The mixing of the phases was visible for every transition on only one recorded pattern (here 540 K and 710 K). As the recording temperatures were the same, whatever the real transition temperature, it may be that a very small amount of second phase is still visible in the following pattern.

Logically, the refined cell parameters show a more symmetrical cell with increasing temperature. Starting with a monoclinic cell and a small beta distortion, it goes to a tetragonal

unit cell before it shows any real cubic symmetry. This can also be shown with the evolution of the distortion of the cell parameters represented in Figure 8. It decreases slowly in the monoclinic phase, and then an abrupt change occurs at the transition; it decreases again in the tetragonal phase and suddenly disappears in the cubic phase.

Also, with increasing temperature, the volume of the unit cell increased (see Figure 9). Similar abrupt changes, common for first-order phase transitions, were also observed for the other compositions.

Existence of the low-temperature phase

The low-temperature phase, characterized by a rhombohedral symmetry, was very difficult to detect in our samples. It was the main contribution to the pattern only in $K_{0.6}Na_{0.4}NbO_3$ (x=0.6) at 100 K, with a small amount of monoclinic phase. It appeared as a minor phase in $K_{0.58}Na_{0.42}NbO_3$ (x=0.58), and was not visible for lower values of x, as shown in Figure 10. This phase was undetectable when the temperature was increased. It disappeared at 110 K for x=0.58, and at 130 K for x=0.6. For all the temperatures, the monoclinic phase was always present with the rhombohedral phase. Thus, this transition is progressive, and cannot be compared to the monoclinic-tetragonal and tetragonal-cubic transitions.

These observations are in agreement with the hypothesis of rhombohedral clusters growing in a matrix when the temperature decreases, as presented by Attia *et al.* for x=0.5 [17]. However, in our case the observed temperatures for the appearance of the rhombohedral phase were lower (140 K in Attia's case).

Conclusion

Samples of $K_xNa_{1-x}NbO_3$ ($0.4 \leq x \leq 0.6$) were prepared by mixing and annealing $KNbO_3$ and $NaNbO_3$. A thermal treatment at 1100°C for 4 hours gave pure phases. At room

temperature the unit-cell parameters of all the samples were refined in monoclinic symmetry with a beta angle close to 90°, and the results confirmed their correct composition. When increasing the temperature, two first-order transitions occurred, leading to tetragonal and cubic phases. At 100 K a rhombohedral phase could be seen, but only in potassium-rich compositions. This phase was only detectable in a narrow range of temperatures, and it was always present with the monoclinic phase. According to our results there was no major change of symmetry in the investigated compositional range, which should be a characteristic of the morphotropic phase-boundary region.

References

1. L. Egerton, D.M. Dillon, J. Am. Ceram. Soc. 42(9) (1959) 438-442.

2. D.H. Cho, M.K. Ryu, S.S.Park, S.Y: Cho, J.G. Choi, M.S. Jang, J.P. Kim, C.R: Cho, J. Korean Phys. Soc., 46 (2005) 151-154.

3. Jaffe, B., Cook, W., Jaffe, H., Piezoelectric ceramics, Academic Press Ltd (1971).

4. V.J. Tennery, K.W. Hang, J. Appl. Phys., 39 (10) (1968) 4749-4753.

5. M. Ahtee, A.W.Hewat, Acta Cryst. A31, (1975) 846-850.

6. M. Uniyal, K. Singh, S. Bhatt, S.C. Bhatt, R.P. Pant, D.K. Suri, B.S. Semwal, Indian J. Pure Appl. Phys., 41 (2003) 305-309.

7. K. Singh, V. Lingwall, S.C. Bhatt, N.S. Panwar, B.S. Semwal, Mater. Res. Bull., 36 (2001) 2365-2374.

8. S. Y. Chu, W. Water, Y. D. Juang, J. T. Liaw, Ferroelectrics, 287 (2003) 23-33.

9. G. Shirane, R. Newnham, R. Pepinsky, Phys Rev, 96 (3) (1954), 581-588.

10. Yosuke Shiratori, Arnaud Magrez 1, Christian Pithan, J. Europ. Ceram. Soc. 25 (2005) 2075–2079.

11. C. Pithan, Y. Shiratori, J. Dornseiffer, F. H. Haegel, A. Magrez, R. Waser, J. Cryst. Growth, 280 (2005) 191-200.

12. M. Ahtee, A.M. Glazer, Ferroelectrics, 7 (1974) 93-95.

13. M. Ahtee, A.M. Glazer, Acta Cryst A32, (1976) 434-446.

14. T. Takeda, Y. Takahashi, N. Wada, Y. Sakabe, Jpn. J. Appl. Phys., 42 (2003) 6023-6026.

15. E. Irle, R. Blachnik, B. Gathier, Thermochimica Acta, 179 (1991) 157-169.

16. V. Petricek, M. Dusek, L. Palatinus, Jana2000. The crystallographic computing system, Institute of Physics, Praha, Czech Republic, (2000).

17. J. Attia, L. Bellaiche, P. Gemeiner, B. Dkhil, B. Malic, J. Phys. IV France, 128 (2005) 55-60.

18. R.D. Shannon, Acta Cryst., A32 (1976) 751-767.

Tables and figures

Table 1: Unit-cell parameters of $K_xNa_{1-x}NbO_3$ with x= [0.4-0.6] at room temperature.

Potassium ratio (%)	a (Å)	b (Å)	c (Å)	Beta (°)	Volume (Å^3)
40	3.99628(4)	3.93776(3)	3.99335(5)	90.3398(5)	62.840(1)
42	3.99854(4)	3.93931(3)	3.99540(4)	90.3400(5)	62.932(1)
44	4.00024(4)	3.94069(3)	3.99713(4)	90.3389(5)	63.009(1)
46	4.00180(4)	3.94202(3)	3.99898(4)	90.3384(5)	63.084(1)
47.5	4.00297(4)	3.94315(3)	4.00009(4)	90.3354(5)	63.1377(8)
48	4.00344(5)	3.94350(3)	4.00021(5)	90.3351(6)	63.152(2)
50	4.0046(4)	3.94464(3)	4.00200(5)	90.3327(5)	63.2179(9)
52	4.00658(4)	3.94591(3)	4.00359(4)	90.3305(5)	63.294(1)
54	4.00754(4)	3.94713(3)	4.00498(5)	90.3268(5)	63.3509(9)
56	4.00931(3)	3.94840(3)	4.00650(4)	90.3268(4)	63.4233(8)
58	4.01080(4)	3.94983(3)	4.00800(4)	90.3226(5)	63.4937(9)
60	4.01220(4)	3.95055(2)	4.00980(3)	90.3244(4)	63.5560(7)

Table 2: Phase-transition temperatures in $K_xNa_{1-x}NbO_3$ compounds in the range x= [0.4-0.6].

Composition	Temperature of the first transition (K)	Temperature of the second transition (K)
$K_{0.4}Na_{0.6}NbO_3$	463.7	678.8
$K_{0.42}Na_{0.58}NbO_3$	464.5	680.6
$K_{0.44}Na_{0.56}NbO_3$	466.4	681.3
$K_{0.46}Na_{0.54}NbO_3$	466.9	683.6
$K_{0.475}Na_{0.525}NbO_3$	467.2	683.5
$K_{0.48}Na_{0.52}NbO_3$	466.7	683

$K_{0.5}Na_{0.5}NbO_3$	466.9	681.9
$K_{0.52}Na_{0.48}NbO_3$	468.9	686.6
$K_{0.54}Na_{0.46}NbO_3$	468.6	686.9
$K_{0.56}Na_{0.44}NbO_3$	470.2	687.3
$K_{0.58}Na_{0.42}NbO_3$	471.7	687.1
$K_{0.6}Na_{0.4}NbO_3$	470.5	687.6

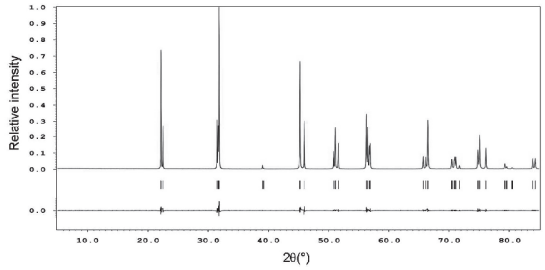

Figure 1: X-ray diffraction diagram of $K_{0.5}Na_{0.5}NbO_3$. The experimental diagram is on the top, the difference diagram is at the bottom, and the tick marks correspond to the refined positions of the peaks.

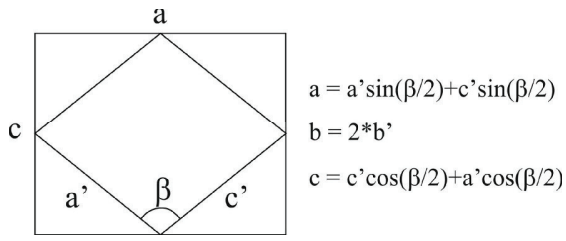

Figure 2: Relationship between orthorhombic (a, c) and monoclinic (a', c', β) unit cells of KNN.

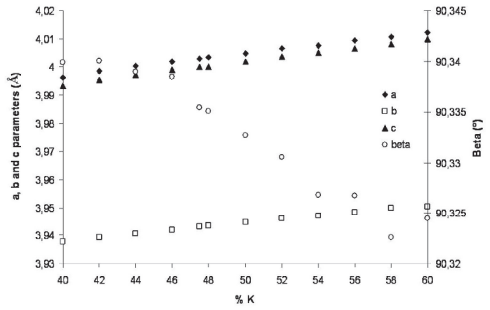

Figure 3: Evolution of the unit-cell parameters of $K_xNa_{1-x}NbO_3$ compounds in the range x= [0.4-0.6].

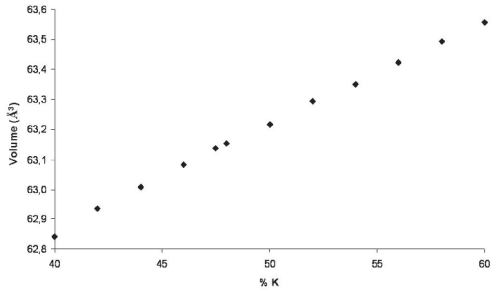

Figure 4: Evolution of the unit-cell volume with the composition of the $K_xNa_{1-x}NbO_3$ compounds in the range x= [0.4-0.6].

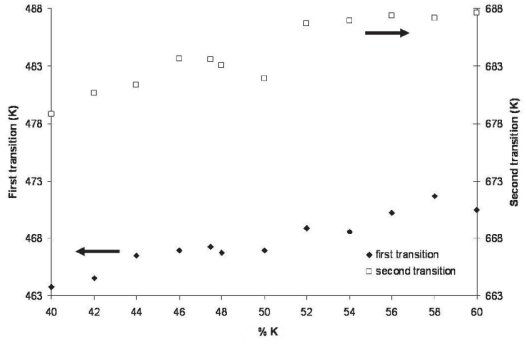

Figure 5: Evolution of the temperatures of the transitions of $K_xNa_{1-x}NbO_3$ compounds in the range x= [0.4-0.6] measured by DSC.

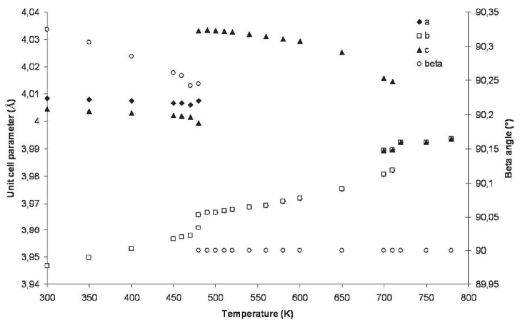

Figure 6: Evolution of the unit-cell parameters with increasing temperature for the composition $K_{0.56}Na_{0.44}NbO_3$.

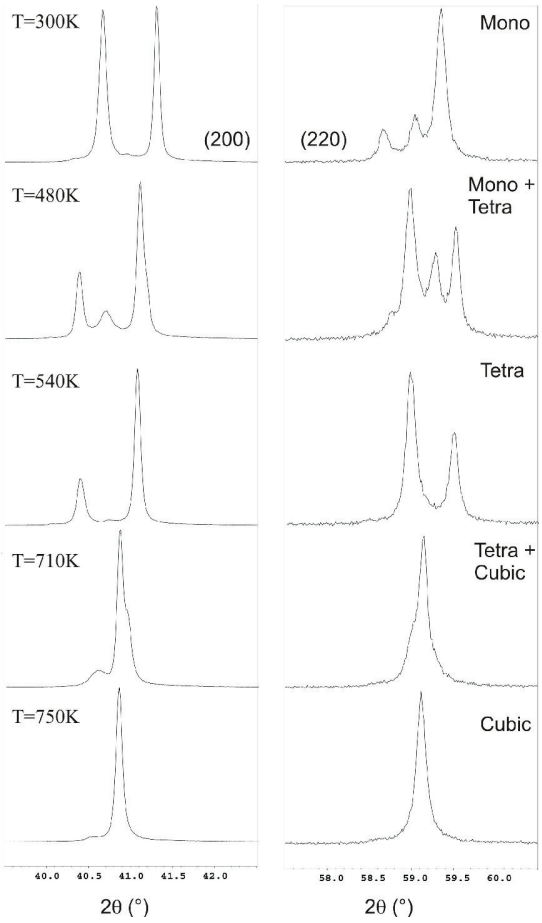

Figure 7: (200) and (220) families of reflections represented at different temperatures, for composition $K_{0.56}Na_{0.44}NbO_3$. The monoclinic, tetragonal and cubic phases are identified, and the mixing of the two phases is clearly visible at the transition temperatures.

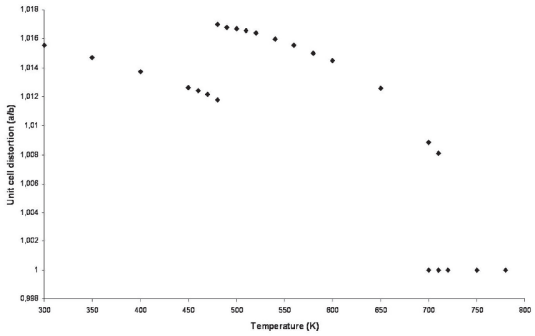

Figure 8: Evolution of the tetragonal distortion with increasing temperature for the composition $K_{0.56}Na_{0.44}NbO_3$.

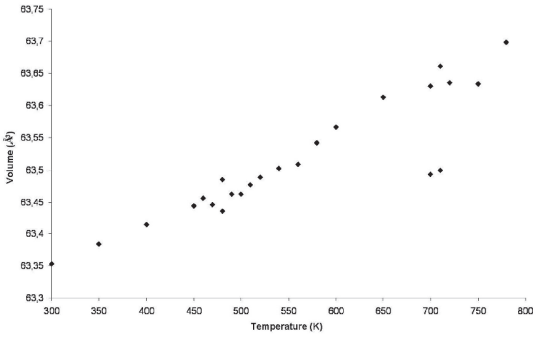

Figure 9: Evolution of unit-cell volume with increasing temperature for the composition $K_{0.56}Na_{0.44}NbO_3$.

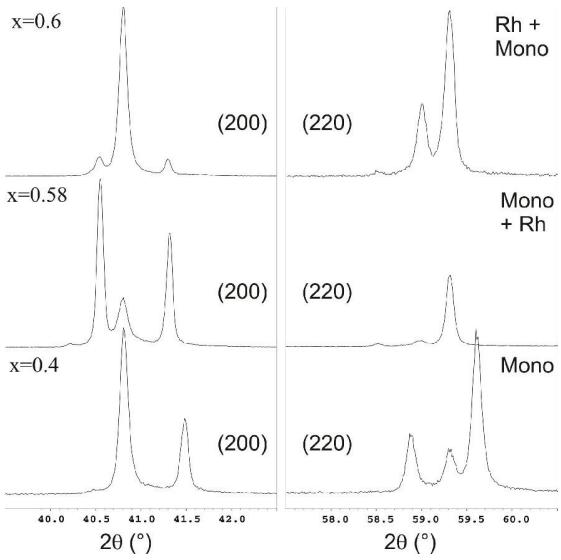

Figure 10: (200) and (220) families of reflections represented at 100K for different compositions of $K_xNa_{1-x}NbO_3$ (x=0.4, x=0.58 and x=0.6). We can see mainly the rhombohedral phase for x=0.6, a mixing of rhombohedral and monoclinic phases for x=0.58, and only the monoclinic phase for lower values of x (x=0.4 in the figure).

Figure
Click here to download high resolution image

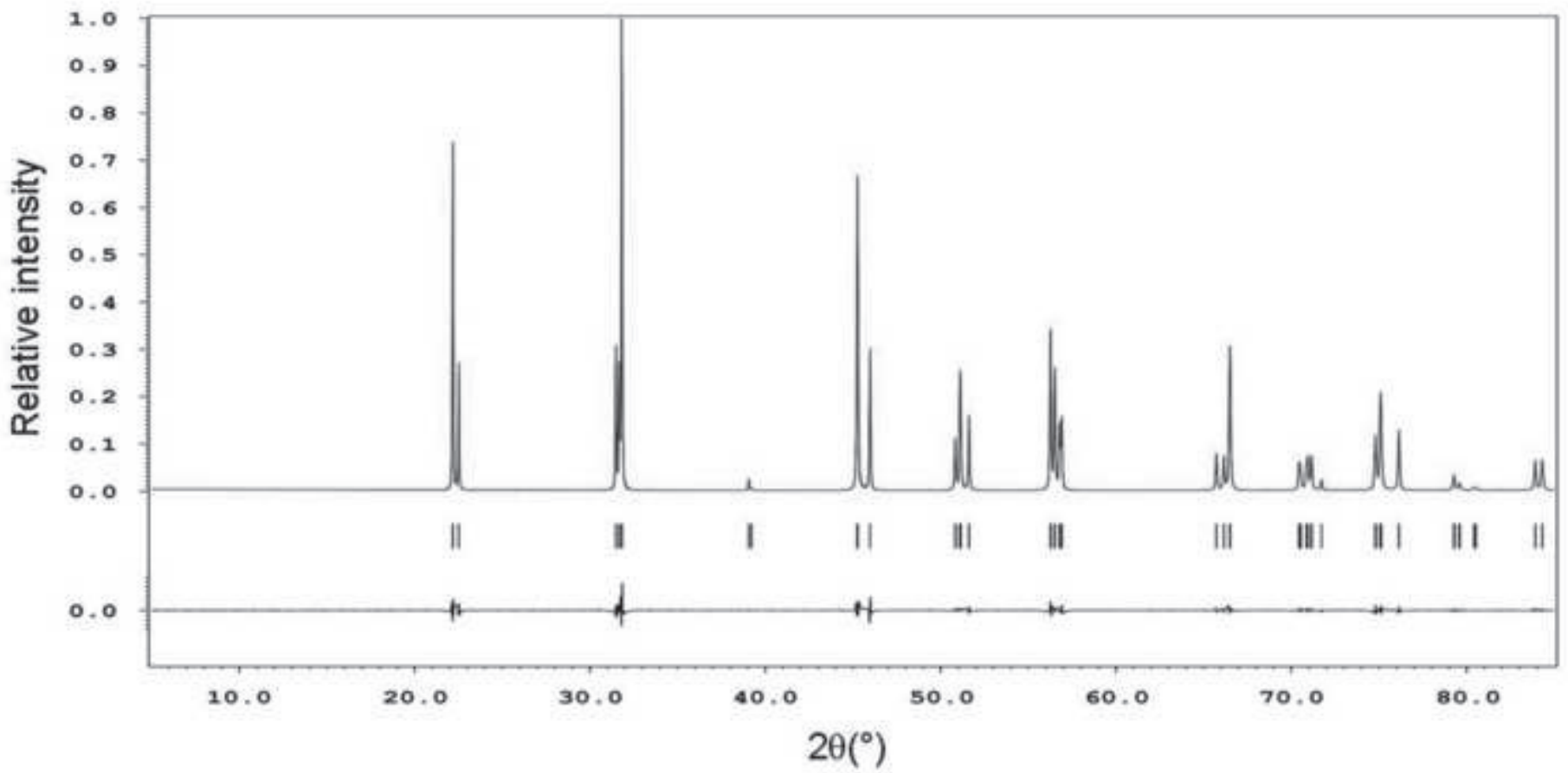

Figure
Click here to download high resolution image

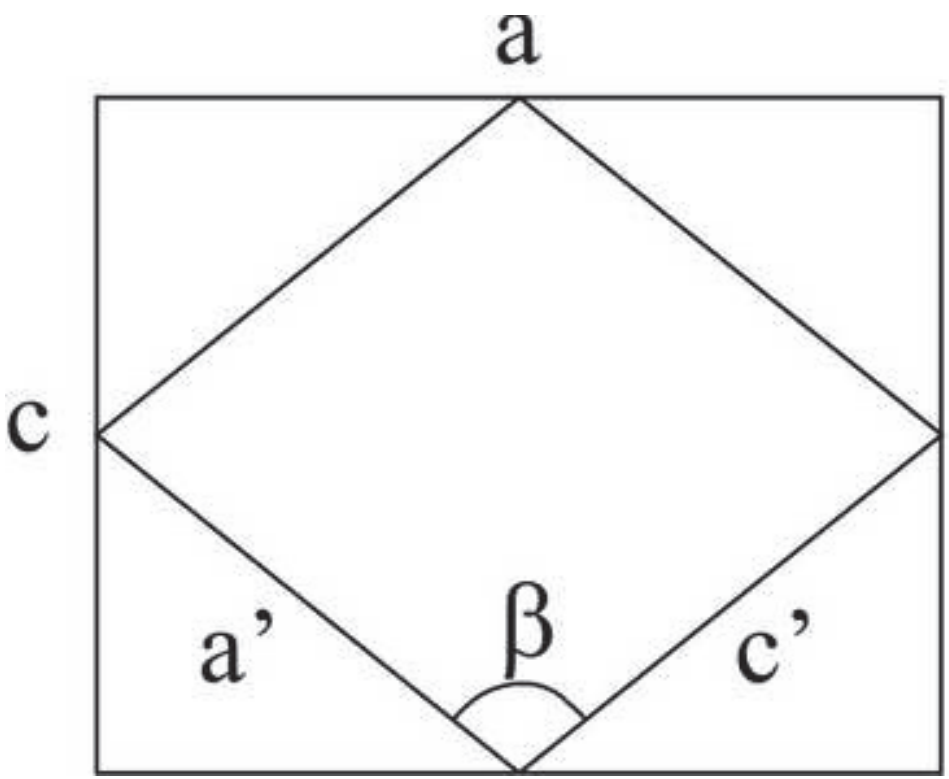

$$a = a'\sin(\beta/2)+c'\sin(\beta/2)$$

$$b = 2*b'$$

$$c = c'\cos(\beta/2)+a'\cos(\beta/2)$$

Figure
Click here to download high resolution image

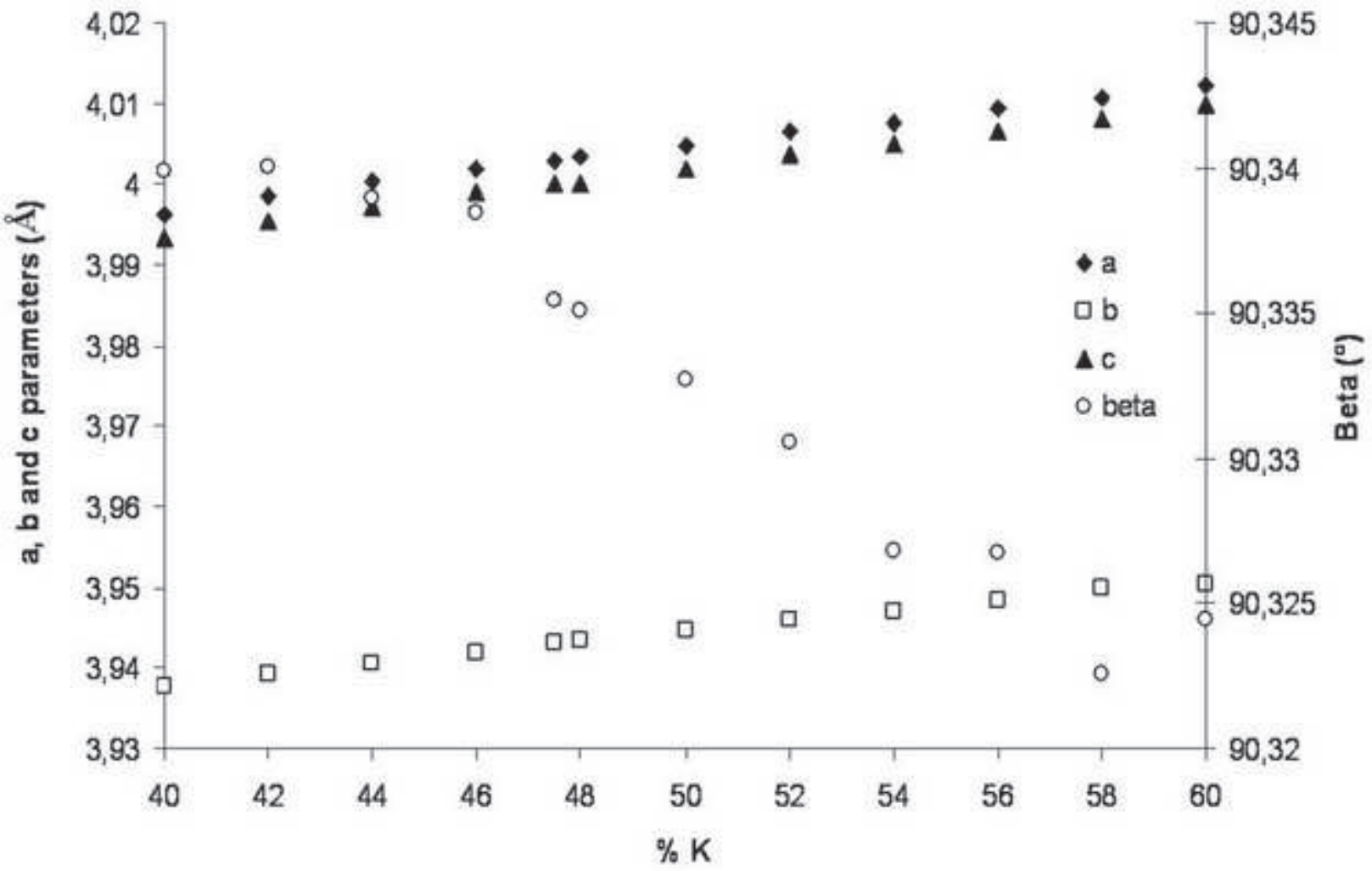

Figure
Click here to download high resolution image

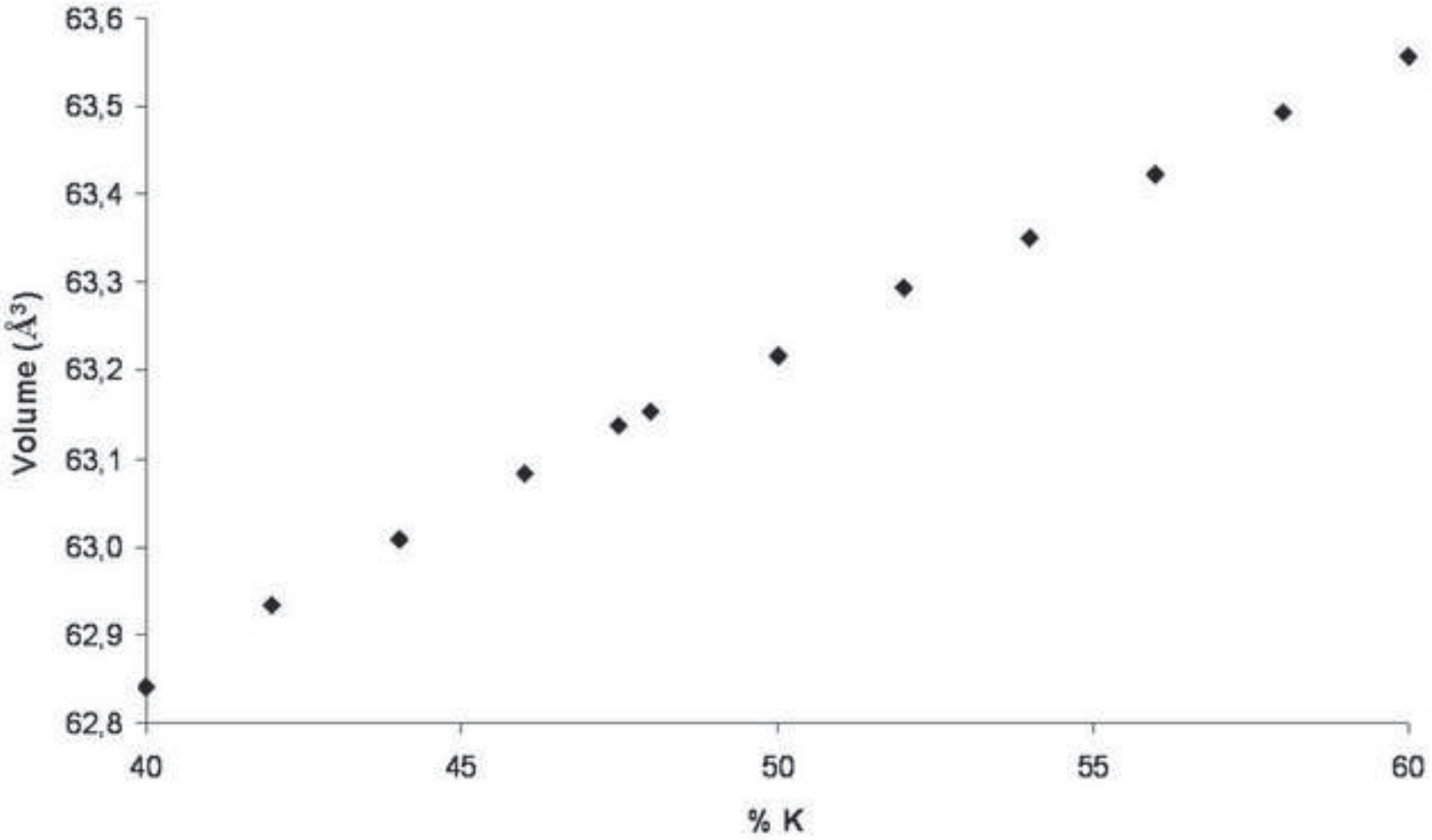

Figure
Click here to download high resolution image

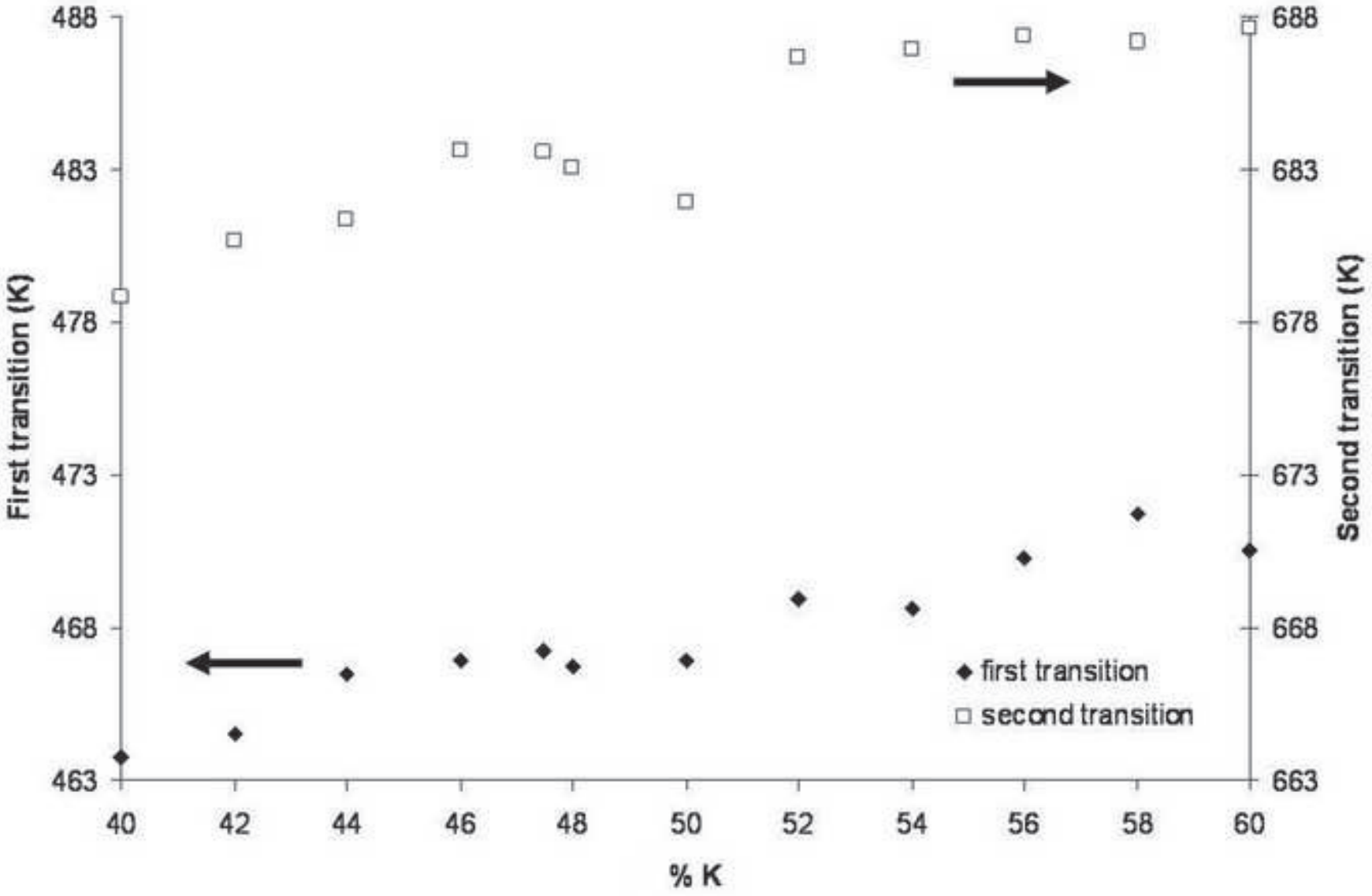

Figure
Click here to download high resolution image

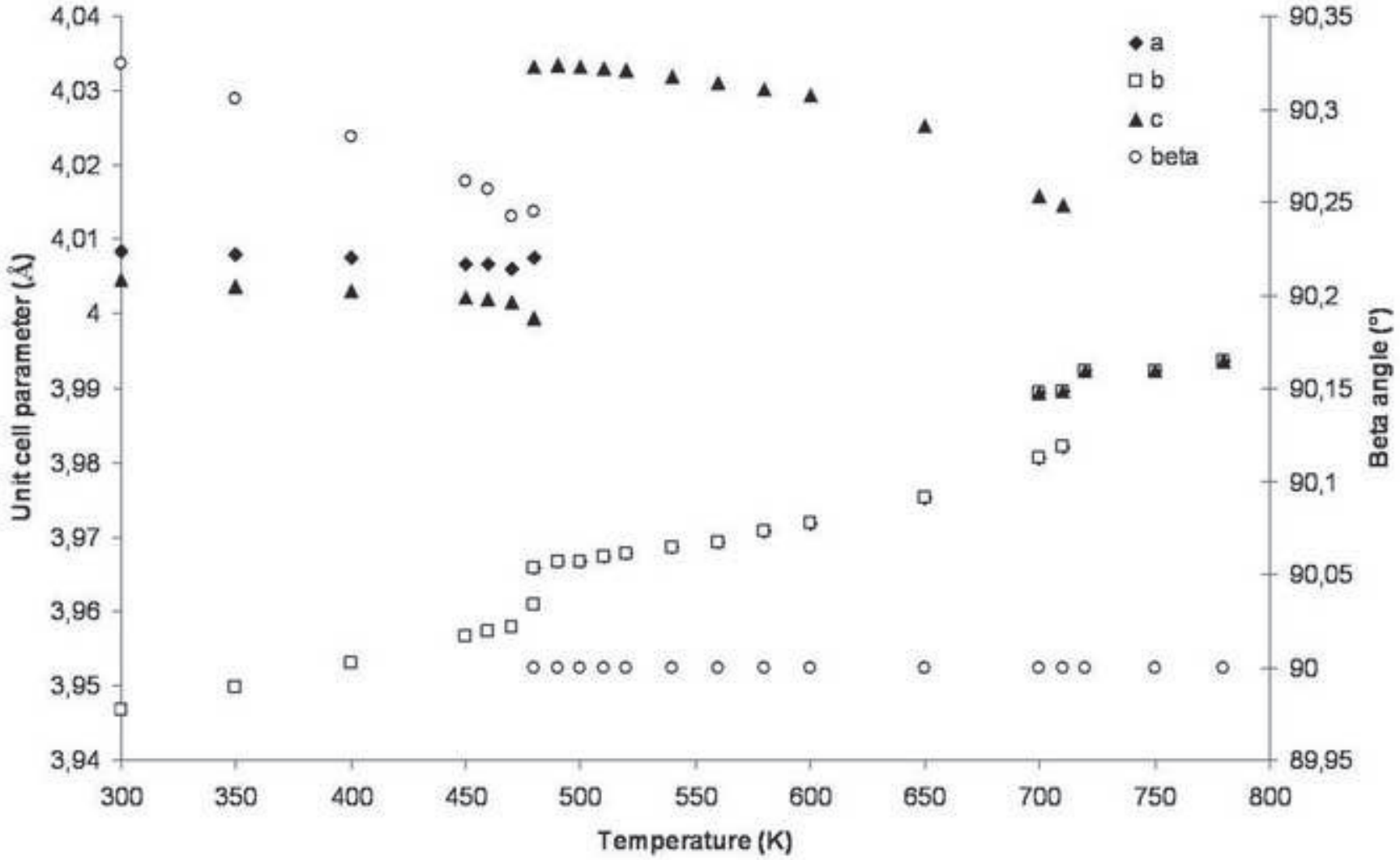

Figure

Click here to download high resolution image

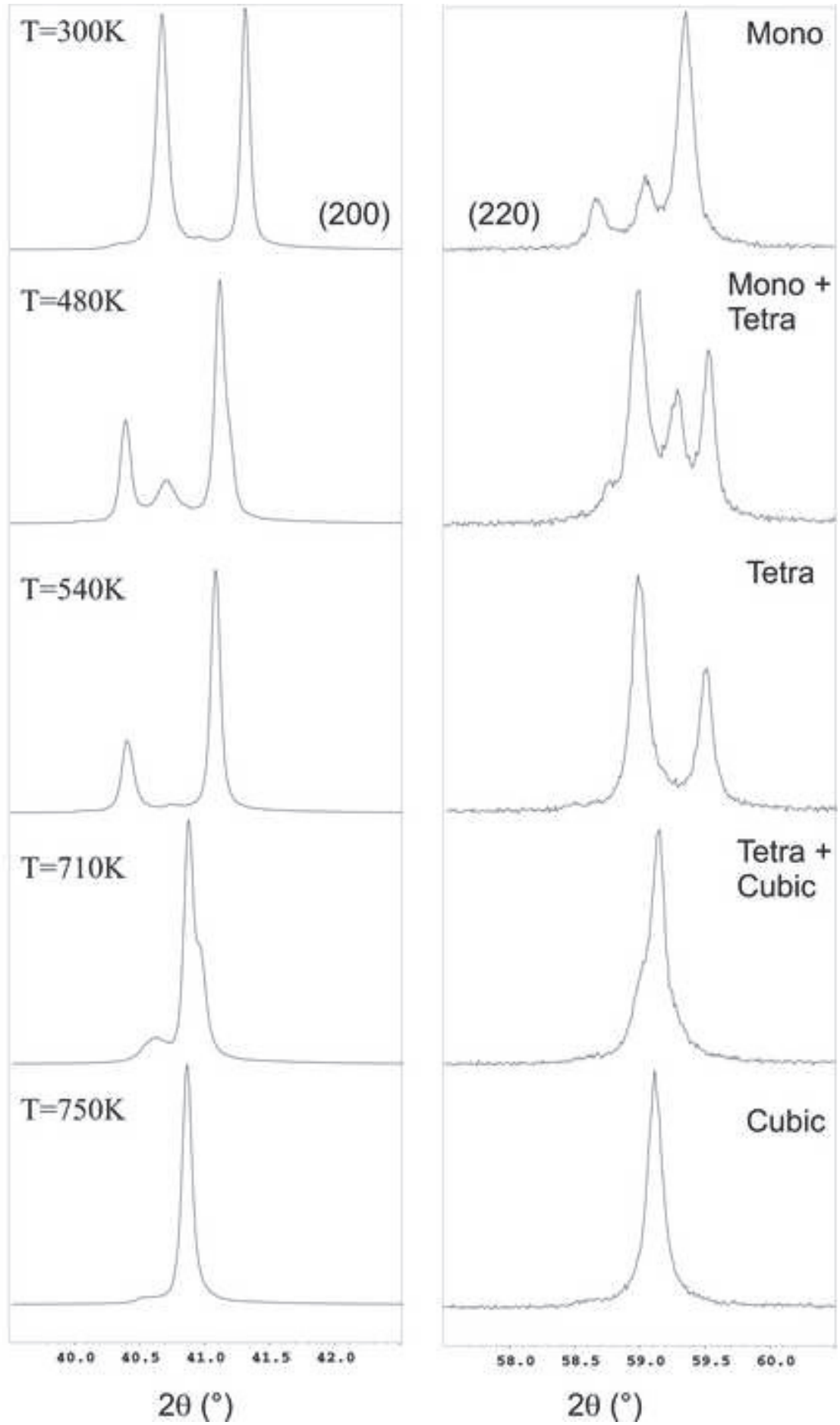

Figure
Click here to download high resolution image

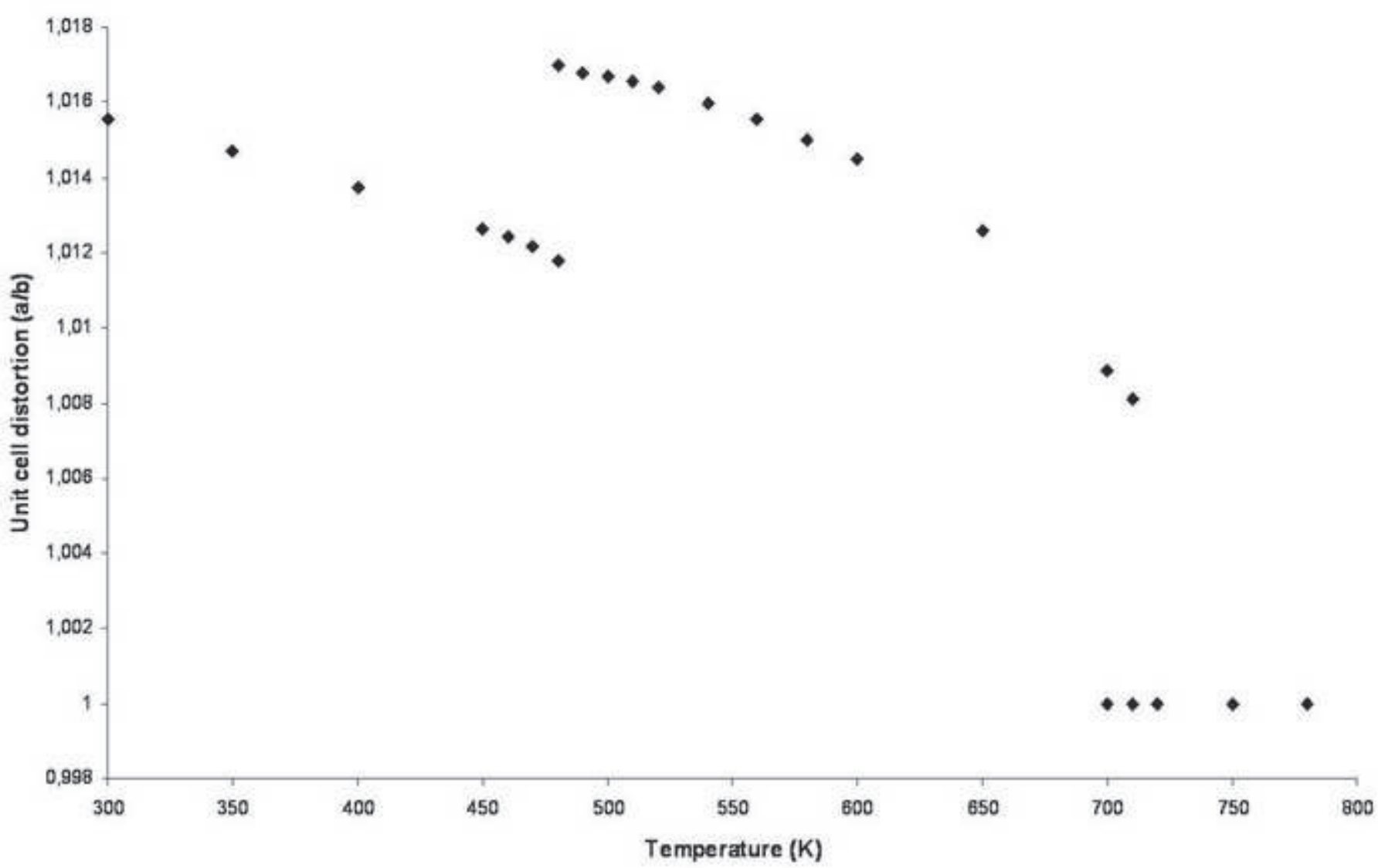

Figure

Click here to download high resolution image

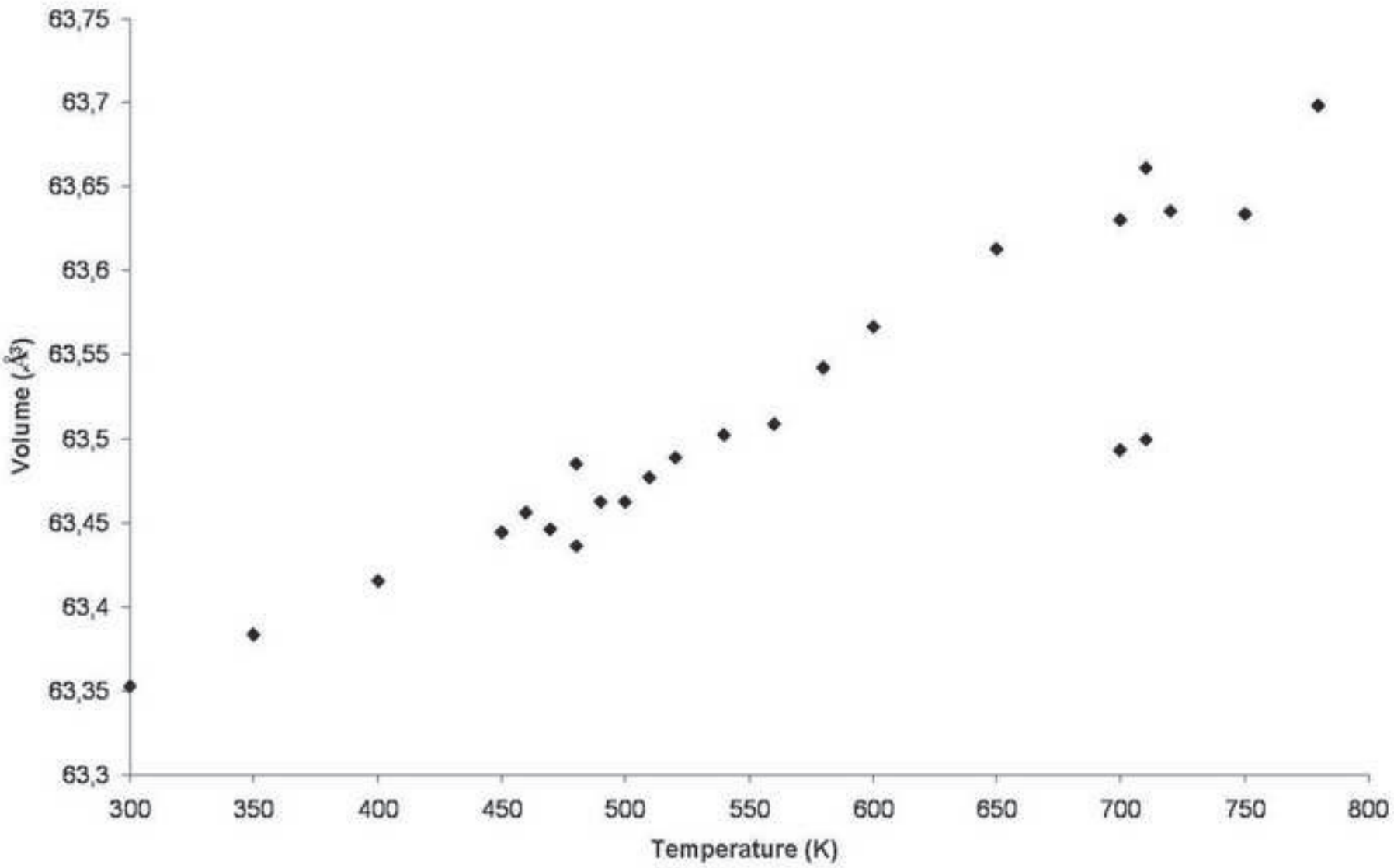

Figure

Click here to download high resolution image